Astron. Astrophys. 352, 19–31 (1999)

ASTRONOMY AND ASTROPHYSICS

Optical and radio behaviour of the blazar S4 0954+65

C.M. Raiteri[1], M. Villata[1], G. Tosti[2], M. Fiorucci[2], G. Ghisellini[3], L.O. Takalo[4], A. Sillanpää[4], E. Valtaoja[4], H. Teräsranta[5], M. Tornikoski[5], M.F. Aller[6], H.D. Aller[6], G. De Francesco[1], P. Heinämäki[4], S. Katajainen[4], L. Lanteri[1], K. Nilsson[4], T. Pursimo[4], N. Rizzi[2], and G. Sobrito[1]

[1] Osservatorio Astronomico di Torino, Strada Osservatorio 20, 10025 Pino Torinese, Italy
[2] Cattedra di Astrofisica, Università di Perugia, Via A. Pascoli, 06100 Perugia, Italy
[3] Osservatorio Astronomico di Brera, Via Bianchi 46, 23807 Merate, Italy
[4] Tuorla Observatory, 21500 Piikkiö, Finland
[5] Metsähovi Radio Observatory, Metsähovintie 114, 02540 Kylmälä, Finland
[6] Department of Astronomy, Dennison Bldg., U. Michigan, Ann Arbor, MI 48109, USA

Received 21 December 1998 / Accepted 6 October 1999

Abstract. We present the results of an intensive optical and radio monitoring of the γ-loud blazar S4 0954+65 from November 1994 to May 1998. The optical observations were done at the Torino, Perugia, and Tuorla Astronomical Observatories; in this period, including two pointings by the Energetic Gamma Ray Experiment Telescope (EGRET), the source was very active and reached its historical maximum. Intranight variability was checked during several nights, giving a positive answer. Colour-index variations were also detected, but no definite trend with brightness can be recognized. The radio light curves at 22 and 37 GHz from the Metsähovi Radio Observatory and those at 4.8 and 14.5 GHz from the University of Michigan Radio Astronomy Observatory (UMRAO) are not well sampled; however, two interesting fast-variability events are present, from which brightness temperatures exceeding the Compton limit by several orders of magnitude can be calculated. A comparison of the optical data with the radio ones does not lead to meaningful results because of the poor radio sampling. Finally, we analyse the spectral energy distributions (SEDs) from the radio to the optical band using contemporaneous radio and optical data taken during two different optical states, with a low radio flux corresponding to the high optical state and vice versa. We first fit these SEDs by means of a helical-jet model, which suggests that the observed large, long-term variations can be due to changes of the jet orientation with respect to the line of sight. Then we fit the same SEDs with a homogeneous model, which can account for the high-energy part of the SED, stressing that external soft photons in addition to the local ones are required to explain the γ-ray data.

Key words: galaxies: active – galaxies: BL Lacertae objects: general – galaxies: BL Lacertae objects: individual: S4 0954+65 – galaxies: jets

Send offprint requests to: C.M. Raiteri
Correspondence to: raiteri@to.astro.it

1. Introduction

Blazars, namely BL Lacertae objects and flat-spectrum radio quasars, are a subclass of active galactic nuclei (AGNs) characterized by flat radio spectra, high and variable polarization, and rapid and large variability at all frequencies.

In the last years an intense observational and theoretical effort has been spent in order to better understand the physical mechanisms responsible for the variable emission of these objects.

From the observational point of view, international monitoring campaigns have been organized, involving both ground and space observatories, with the aim of covering the whole electromagnetic spectrum, from the radio to the γ-ray band. In particular, with the launch of the Compton Gamma Ray Observatory (CGRO) in 1991, a lot of new γ-ray data in the $0.5\,\mathrm{MeV}$ – $30\,\mathrm{GeV}$ energy range has become available, and one of the most important discoveries has been that blazars emit a substantial fraction of their power at γ-ray energies.

The spectral energy distribution (SED) of blazars is currently explained in terms of two components: the first one, which accounts for the emission from the radio to the X-ray band, is synchrotron emission from relativistic electrons in a magnetized plasma, while the higher-energy emission is likely to be inverse-Compton radiation from soft photons produced internally to the plasma (the synchrotron photons) or externally to it and upscattered by the synchrotron emitting electrons. Various models for the emitting plasma have been proposed and the observations have not been able to favour one of them in particular yet.

In this paper we present observations of the blazar S4 0954+65 in the $BVRI$ bands performed at the Torino, Perugia, and Tuorla Astronomical Observatories during the last four observational seasons, together with observations at 22 and 37 GHz from the Metsähovi Radio Observatory and at 4.8 and 14.5 GHz from the University of Michigan Radio Astronomy Observatory (UMRAO). The aim of this collaboration has been to obtain a dense sampling to better know the emission properties of this source. In particular, during the first observational

season the purpose was also to provide the optical counterpart to the Energetic Gamma Ray Experiment Telescope (EGRET) observations, in order to detect possible correlations between the emissions in the two bands. This is the first time that such a large database is constructed for this source, allowing to study the emission features both on the long and on the short time scales.

In Sect. 2 we present the object S4 0954+65, giving a brief review of the most important observational results previously published. Details on the observation and data reduction techniques are given in Sect. 3, where the calibration of a $BVRI$ photometric sequence is also presented. The light curves during the four observational seasons are described in Sect. 4, while intranight and colour-index variations are discussed in Sects. 5 and 6, respectively. In Sect. 7 the radio data from the Metsähovi Radio Observatory and from the UMRAO database are presented and two noticeable fast-variability episodes are discussed; in the following section SEDs with radio and optical contemporaneous data are constructed and fitted by means of both a helical-jet model and a homogeneous one. The latter model is also used to fit the high-energy portion of the SED. The main conclusions of this work are finally drawn in Sect. 9.

2. The blazar S4 0954+65

The object S4 0954+65 was first identified as a radio source during the Jodrell-Bank $996\,\mathrm{MHz}$ Survey, and its optical counterpart was found by Cohen et al. (1977). Walsh et al. (1984) classified S4 0954+65 as a BL Lac object from the analysis of its spectrum, showing a smooth continuum with no detectable emission or absorption features.

The source belongs to the $1\,\mathrm{Jy}$ catalogue of radio sources (Kuhr et al. 1981) and was included in the complete sample of $1\,\mathrm{Jy}$ radio-selected BL Lac objects (RBLs) by Stickel et al. (1991). VLA images show a curved jet extending south on arcsec scales (Kollgaard et al. 1992). VLBI maps reveal a strongly polarized core and jet components with an unusually high superluminal motion, whose polarization is not so well aligned with the VLBI structural axis as is typical for BL Lacertae objects: this suggests that also the milliarcsecond jet is curved (Gabuzda et al. 1992, 1994; see also Gabuzda & Cawthorne 1996).

A flatter energy distribution than usually observed in RBLs was discovered in both the ROSAT X-ray band (Comastri et al. 1995, 1997; Urry et al. 1996) and the EGRET γ-ray band (Mukherjee et al. 1995). Some authors (see e.g. Kollgaard et al. 1992; Comastri et al. 1995; Sambruna et al. 1996) suggested that S4 0954+65 may be a transition object whose behaviour is intermediate between those of BL Lacs and flat-spectrum radio quasars (FSRQs).

The first measurement of the redshift of S4 0954+65 was made by Lawrence et al. (1986). They obtained $z = 0.368$ from some galactic absorption lines present in the spectrum. This value was then confirmed by Stickel et al. (1993), who found $z = 0.367$ based on a spectrum that, in addition to the galactic absorption lines, showed also an extremely weak emission line.

The host galaxy of S4 0954+65 is unresolved in the image reported by Stickel et al. (1993). The compactness of this source has been confirmed also by the high-resolution images obtained by Wurtz et al. (1996), who classified the host galaxy as a marginally resolved elliptical galaxy. Close to this BL Lac there are two very faint galaxies having redshifts of 0.315 and 0.039 (Stickel et al. 1993).

Cohen et al. (1977) estimated the apparent optical magnitudes from the red and blue Palomar Sky Surveys. These authors found $R = 16.7$ and $B = 17.8$, with an error of about $0.5\,\mathrm{mag}$ in both bands. It is worth noting that the V magnitude reported by Véron & Véron (1993) is actually the R value estimated by Cohen et al. (1977). A more recent value for the V magnitude of S4 0954+65 can be found in the compilation of BL Lac objects by Padovani & Giommi (1995), who report $V = 17.0$.

The variability of S4 0954+65 in the optical band was studied by Wagner et al. (1990, 1993) and Heidt & Wagner (1996). These works were mainly devoted to detecting intraday variability; therefore the source was intensively observed only for short periods of time, using differential photometry in the Johnson's R band. In particular, Wagner et al. (1990, 1993) performed also coordinated observations in the radio band. The result of these works is that S4 0954+65 presents intraday variability of both its optical and radio emissions, with a possible correlation between them.

Other radio observations of S4 0954+65 were done by Waltman et al. (1991) and Quirrenbach et al. (1992). The radio flux shows variations of the order of 30–50% on time scales of months, together with the above mentioned intraday variations of smaller amplitude. An unusual minimum in the light curve at $2.7\,\mathrm{GHz}$ and contemporaneous strong spikes at $8.1\,\mathrm{GHz}$ were registered in 1981; these features were explained as due to an extreme scattering event (Fiedler et al. 1987).

The source was observed in the infrared by the IRAS satellite, covering the 12–$100\,\mu\mathrm{m}$ band (Impey & Neugebauer 1988), in the X-ray band between 0.1 and $2.4\,\mathrm{keV}$ by the ROSAT satellite (Comastri et al. 1995, 1997; Urry et al. 1996), and in the γ-ray band, above $100\,\mathrm{MeV}$, by EGRET (Mukherjee et al. 1995, 1997). It has been indicated by the Chicago Air Shower Arrays – Michigan Muon Array (CASA–MIA) experiment as a possible AGN emitting at energy $\gtrsim 10^{14}\,\mathrm{eV}$, but no evidence of ultrahigh-energy emission has been recorded (Catanese et al. 1996).

3. Observations

3.1. Optical observations

The photometric observations were carried out with the $1.05\,\mathrm{m}$ astrometric telescope of the Torino Observatory, the $0.4\,\mathrm{m}$ Automatic Imaging Telescope of the Perugia University Observatory (Tosti et al. 1996), and the $1.03\,\mathrm{m}$ telescope of the Tuorla Observatory. The telescopes were equipped with CCD cameras and standard BV (Johnson) and RI (Cousins) filters. Data reduction was performed with the standard IRAF plus locally developed procedures. The comparison among the data obtained in the same nights with different telescopes showed a general

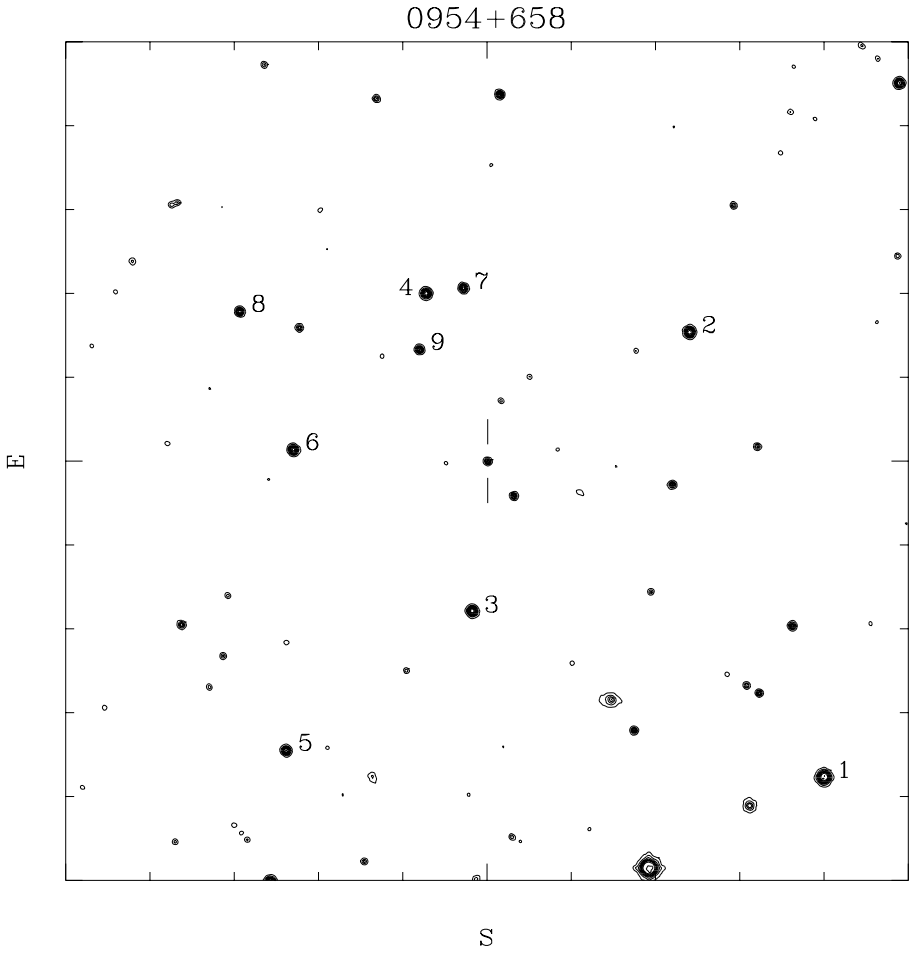

Fig. 1. Finding chart of the field of S4 0954+65 (adapted from the STScI Digitized Sky Survey); north is up and east on the left; the squared box is $10\,\mathrm{arcmin}$ wide

Table 1. $BVRI$ magnitudes of the comparison stars

Star	B	V	R	I
1	13.58±0.02	12.91±0.02	12.56±0.02	
2	15.02±0.02	14.37±0.02	13.96±0.03	13.58±0.05
3	15.45±0.02	14.61±0.02	14.12±0.02	13.67±0.07
4	16.12±0.04	14.94±0.03	14.25±0.03	13.56±0.04
5	16.22±0.02	15.31±0.02	14.85±0.02	
6	16.84±0.02	15.35±0.03	14.43±0.03	13.58±0.05
7	16.60±0.04	15.75±0.02	15.22±0.03	14.73±0.07
8	16.65±0.02	15.85±0.06	15.39±0.04	
9	17.01±0.02	16.17±0.05	15.69±0.02	15.11±0.07

Table 2. Summary of the optical monitoring results

Filter	N.data	max	JD(max)	min	JD(min)
B	109	15.99	2450851.590	17.99	2450459.537
V	128	15.46	2449865.381	17.21	2450459.530
R	292	14.92	2450862.448	16.69	2450459.545
I	111	14.31	2450865.445	15.85	2450400.676

agreement; in the cases where variations were detected they are consistent with the usual variations of the source.

Comparison stars in the field of S4 0954+65 were calibrated in $BVRI$ for the first time during our monitoring campaign using several Landolt's fields (Landolt 1992). They are indicated on the finding chart in Fig. 1; Table 1 reports their $BVRI$ magnitudes.

We monitored the blazar S4 0954+65 during the period November 1994 – May 1998. Table 2 gives some information about our monitoring results: for each filter it reports the total number of observations and the maximum and minimum brightness levels (mag) observed together with their corresponding Julian Date.

3.2. Radio observations

The radio observations at 22 and 37 GHz were done with the $13.7\,\mathrm{m}$ antenna of the Metsähovi Radio Observatory as a part of a long-term continuous monitoring program of AGN started in 1980. The observations were done with standard ON/ON techniques with DR 21 used as a calibration source. The observing procedure and data reduction is described in more detail in Teräsranta et al. (1992).

The source S4 0954+65 is a member of the BL Lac sample monitored at the UMRAO. The observations are made with the University of Michigan $26\,\mathrm{m}$ paraboloid operating at 14.5, 8.0, and $4.8\,\mathrm{GHz}$. Measurements of both total flux density and linear

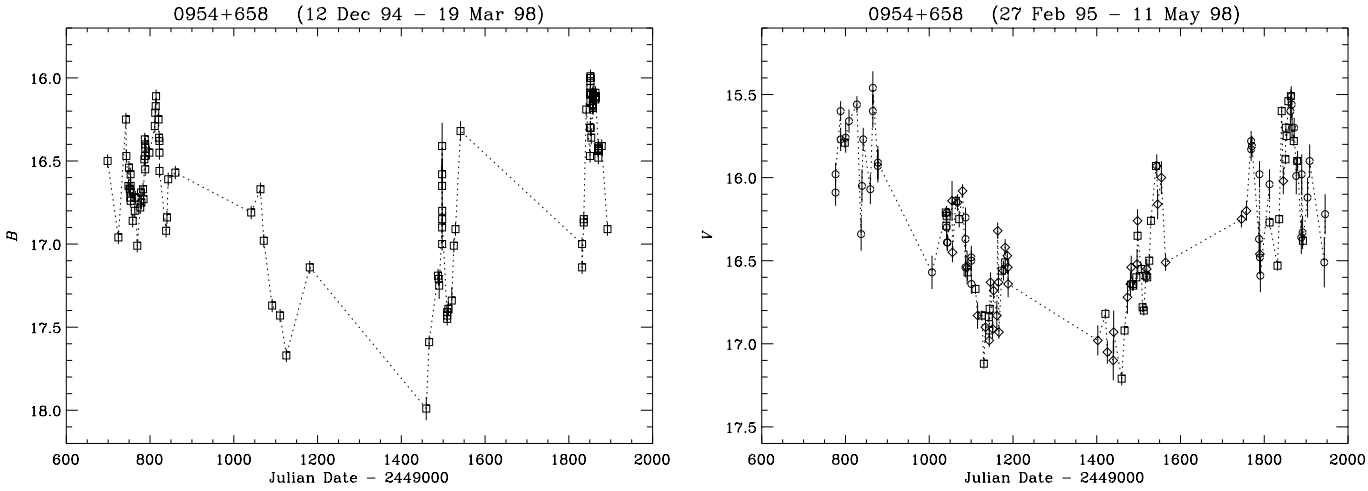

Fig. 2. Light curves of S4 0954+65 in the B (left) and V (right) bands; squares represent data from the Torino Observatory, circles those from the Perugia Observatory, and diamonds those from the Tuorla Observatory

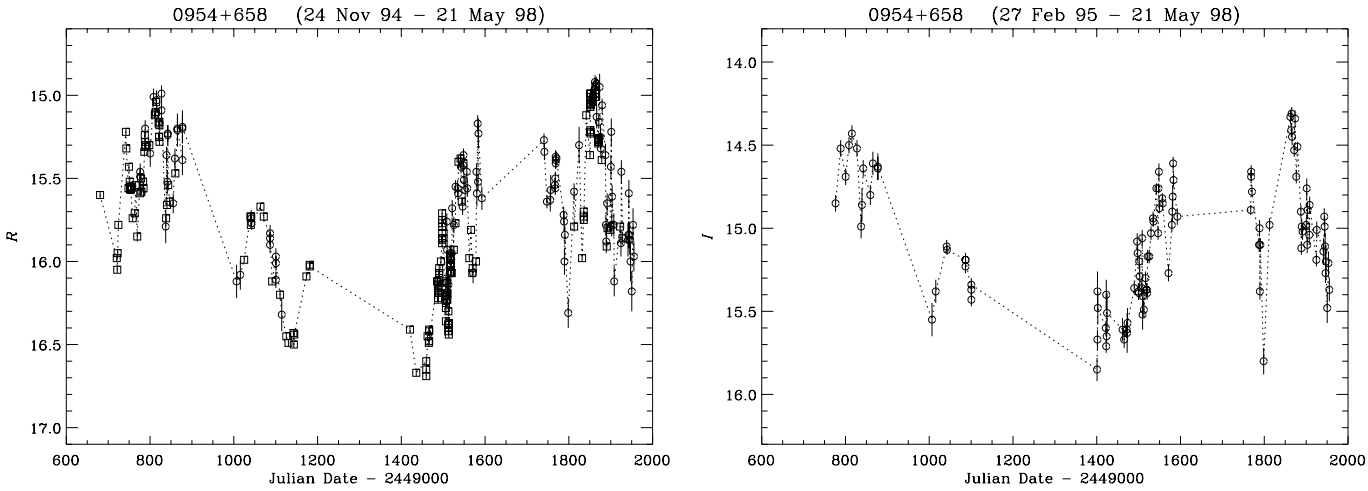

Fig. 3. Light curves of S4 0954+65 in the R (left) and I (right) bands; symbols as in Fig. 2

polarization are obtained. For a description of the observing and data reduction procedures see Aller et al. (1985; see also Aller et al. 1999).

4. Optical light curves

The total light curves in the four bands are presented in Figs. 2 and 3; data from the Torino Observatory are indicated by squares, data from the Perugia Observatory by circles, and data from the Tuorla Observatory by diamonds.

The results of our monitoring campaign during the first observational season, from November 1994 to June 1995, are shown in Fig. 4, where data in the R band, the best sampled one, are presented. From January to June 1995 (JD $=$ 2449720–2449877) the source was observed during an outburst, whose structure is very complex. Our data display two major flares at JD $=$ 2449721–2449769 and JD $=$ 2449769–2449837. During the latter the source peaked at $R = 14.99$ on April 19, 1995. At that time this was the highest brightness level of S4 0954+65 ever observed. Rapid variations with small amplitude and time scales of a few days are superposed to each of these flares.

In the period under consideration the source was pointed by EGRET twice, from February 14 to 28, 1995 (JD $=$ 2449763.20–2449777.14) and from April 25 to May 9, 1995 (JD $=$ 2449833.14–2449846.95). We registered rapid flux variations of some tenths of magnitude during both pointings; unfortunately, the corresponding published γ-ray data are only upper limits (Mukherjee et al. 1997).

Fig. 5 shows the light curve of S4 0954+65 in the V band from October 1995 to April 1996. During this second observational season the source was in a faint state and, after a small brightness increase, a fall of $1.04\,\mathrm{mag}$ in 51 days led the source to $V = 17.12$ on February 16, 1996 (JD $=$ 2450130). From then on, an increasing trend is visible, with many oscillations superimposed.

At the beginning of the third observational season the source was still (or again) in a faint state, and it reached the minimum brightness detected during our monitoring campaign:

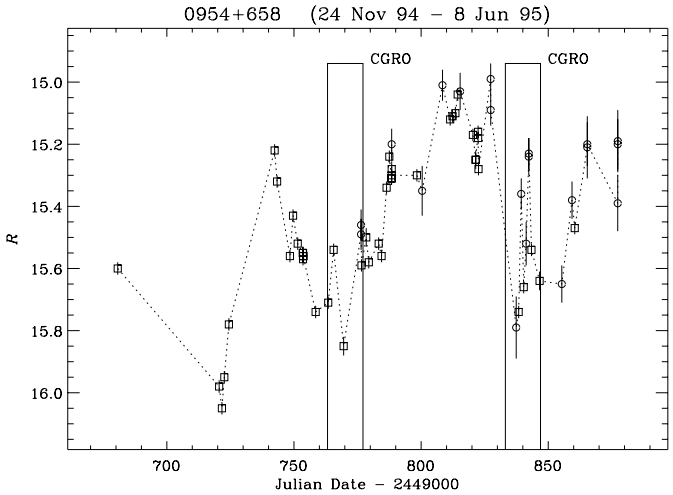

Fig. 4. Light curve of S4 0954+65 in the R band during the first observational season; symbols as in Fig. 2; the two periods corresponding to pointings by EGRET are indicated by boxes

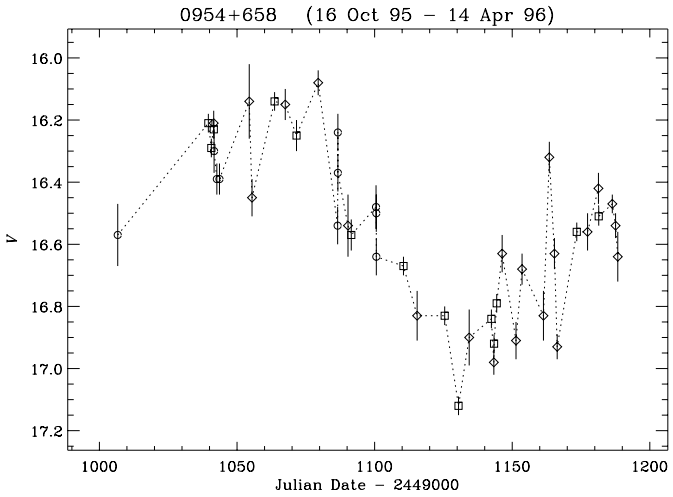

Fig. 5. Light curve of S4 0954+65 in the V band during the second observational season; symbols as in Fig. 2

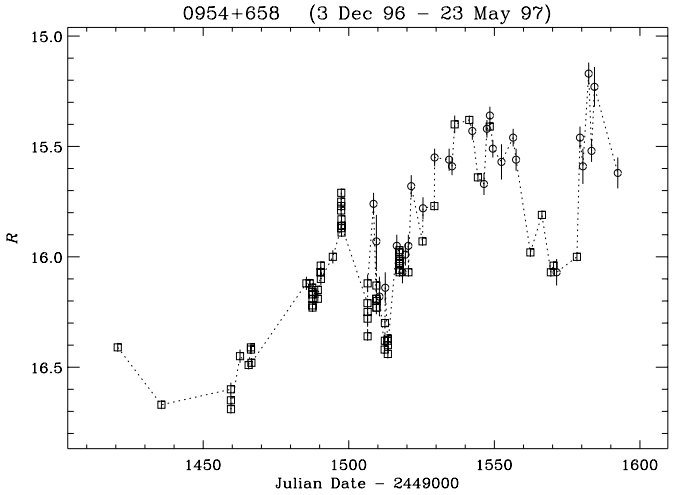

Fig. 6. Light curve of S4 0954+65 in the R band during the third observational season; symbols as in Fig. 2

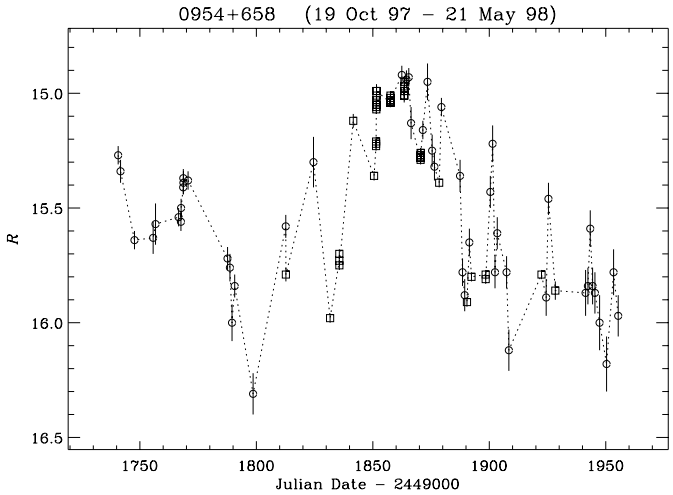

Fig. 7. Light curve of S4 0954+65 in the R band during the fourth observational season; symbols as in Fig. 2

$R = 16.69$ on January 11, 1997 (JD $= 2450459$; see Fig. 6). Then it started to brighten through successive jumps, up to $R = 15.17$ on May 13, 1997 (JD $= 2450582$).

An intense activity was detected during the fourth observational season (see Fig. 7), when a big outburst made the source reach the historical brightness maximum ($R = 14.92$ on February 17, 1998, JD $= 2450862$). Fast and large-amplitude variations were also observed.

5. Intranight variations

The intraday optical variability of the source S4 0954+65 was studied by Wagner et al. (1990, 1993) and Heidt & Wagner (1996). Wagner et al. (1990) discovered the first intraday variability event by observing the source for 10 days during May 1989: flux variations in the R band up to 100% in 20 hours were registered. Wagner et al. (1993) report observations carried out in February 1990; the authors detected several rapid flares during a four-week monitoring program, with a brightness increase of more than a factor 6. Moreover, they found that the shape of these flares was symmetric and similar to one another, suggesting that geometric effects might be responsible for the variations. The existence of short-term variations in the 0954+658 optical emission was then confirmed by Heidt & Wagner (1996) in their statistical analysis of intraday variability in 34 BL Lac objects.

We searched for fast flux variations in several nights during our monitoring program; in a number of cases we took R and B frames in succession in order to investigate also possible colour variations (see the following section).

One of the most interesting cases of intranight variations is that observed in the night of February 6–7, 1998 (JD $=$ 2450851), which is shown in Fig. 8. A brightness increase of 0.24 mag in 4 hours and 53 minutes characterizes the light curve in the R band, while an increase of 0.31 mag in 4 hours and 15 minutes was detected in the B band.

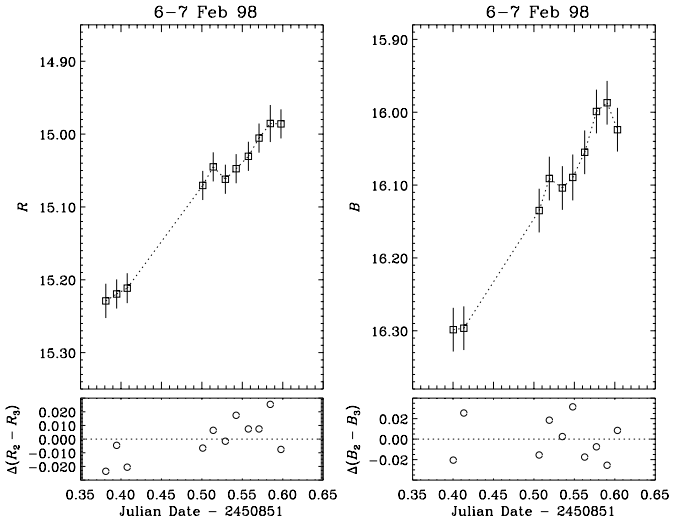

Fig. 8. Light curve of S4 0954+65 in the R and B bands during the night of February 6–7, 1998 (JD $= 2450851$)

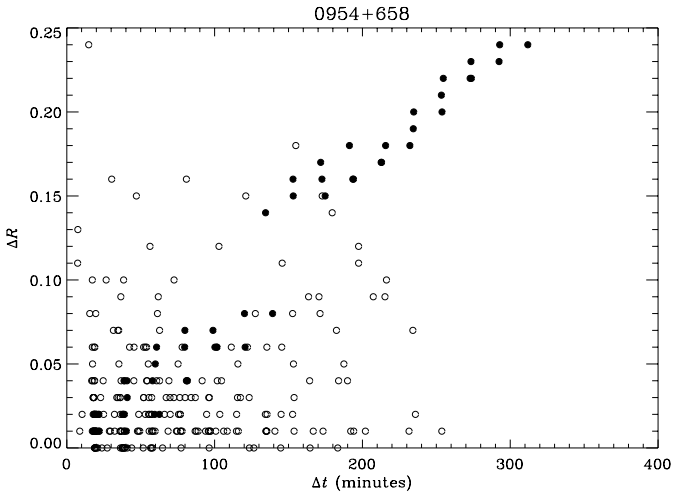

Fig. 9. Difference in R magnitude between frames taken in the same night with the same telescope as a function of their time separation; filled symbols correspond to the night of JD $= 2450851$.

In order to have an idea of what kind of intranight variations were registered, Fig. 9 shows all the differences in the R magnitude between frames taken in the same night with the same telescope as a function of their time separation expressed in minutes. Only nights with more than three R frames were considered. Typical errors are of the order of $0.02\,\mathrm{mag}$. Data corresponding to the night of JD $= 2450851$ are indicated with filled symbols. As one can see, variations $\gtrsim 0.1\,\mathrm{mag}$ were detected on very short time scales.

6. Colour-index variations

In order to see whether there have been changes in the colour index, Fig. 10 shows $B - R$ versus R. All colour indices have been obtained by selecting data from the same observatory and by coupling B and R frames separated by no more than 15 minutes. In the left panel data from the first observational season (squares) are distinguished from those from the third (triangles) and fourth (circles) ones. No $B-R$ colour indices matching the above criteria could be obtained from the second observational season.

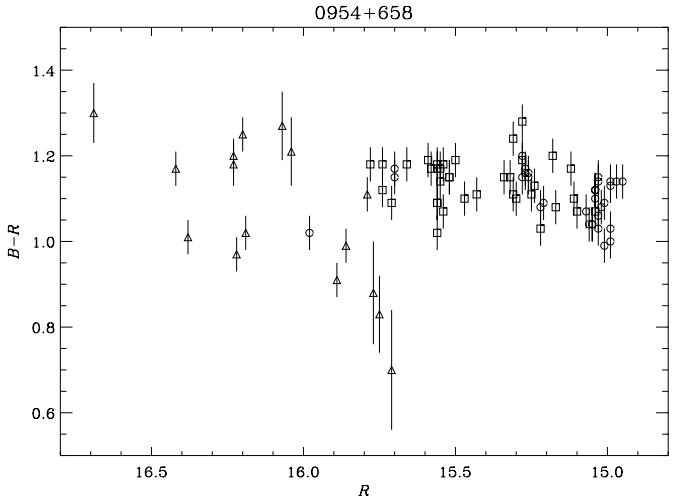

Fig. 10. The colour index $B - R$ plotted versus the R magnitude; squares refer to data of the first observational season, triangles and circles to the third and fourth seasons, respectively

From an inspection of the figure one can see that a larger dispersion characterizes the data of the third season, many of which present big errors that, in turn, reflect the big errors on the B data mainly due to the reflectiveness degrading of the Torino telescope at that time.

The weighted mean of the 85 data plotted in Fig. 10 is $B - R = 1.11$. Eight out of these data present larger than $3\,\sigma$ deviations from the mean and can thus be regarded as the signature of intrinsic colour-index variations. However, no trend with the source brightness can be recognized.

7. Radio light curves

The radio light curves at 37 and 22 GHz from the Metsähovi Radio Observatory in the period of interest are shown in Fig. 11 (middle and bottom panels, respectively). Unfortunately the radio sampling is poor, especially at 37 GHz. The radio data at 14.5 and 4.8 GHz from the UMRAO database are plotted in Fig. 12; also in this case the sampling is not good.

An interesting feature in the 22 GHz light curve is the fast variation observed between November 30 and December 2, 1995: a fall from $1.33 \pm 0.07\,\mathrm{Jy}$ to $0.56 \pm 0.03\,\mathrm{Jy}$ in 50.5 hours. These fluxes have been checked carefully and appear reliable. By taking a redshift value of $z = 0.367$ and assuming $H_0 = 50\,\mathrm{km\,s^{-1}\,Mpc^{-1}}$ and $q_0 = 0.5$, we estimate a distance of $2.4 \times 10^3\,\mathrm{Mpc}$ and a brightness temperature of $5.1 \times 10^{16}\,\mathrm{K}$, which is more than 10^4 times the Compton limit, implying a Doppler factor $\delta \sim 37$. The apparent velocity of the emission blobs estimated by Gabuzda et al. (1994) and Gabuzda & Cawthorne (1996) is $\beta_\mathrm{a} \sim 12$, so that the angle to the line of sight would be about 1°.

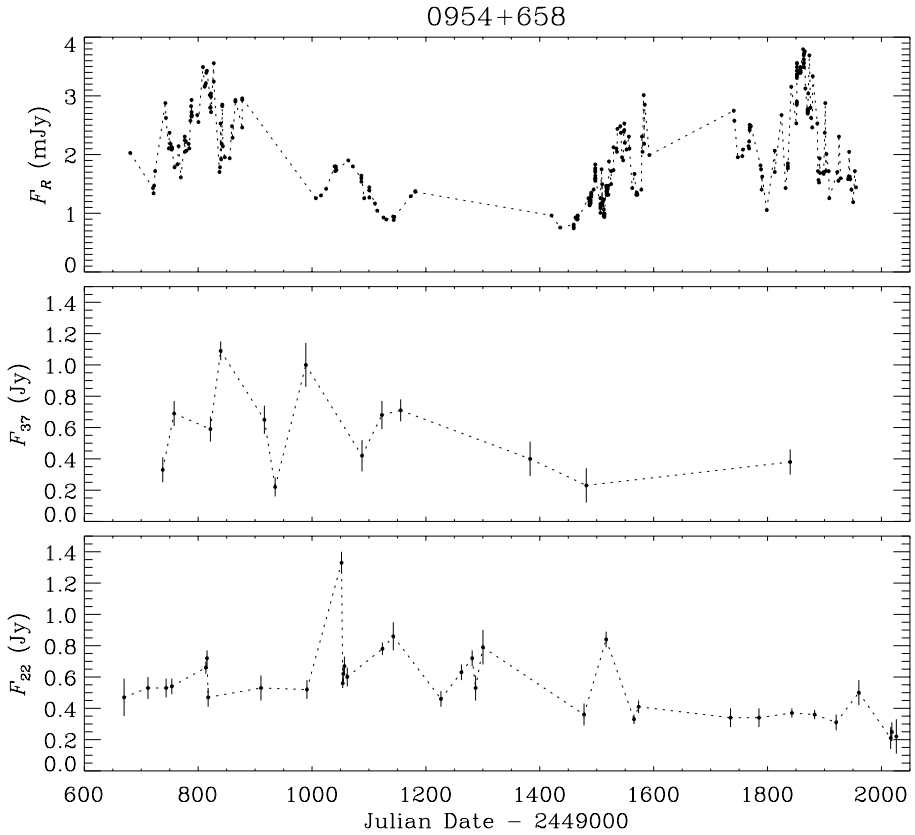

Fig. 11. Confrontation between the optical data in the R band (top panel) and the radio data at 37 GHz (middle panel) and 22 GHz (bottom panel) from the Metsähovi Radio Observatory

Another interesting radio event is the fall from 0.71 ± 0.02 Jy to 0.42 ± 0.02 Jy registered at 14.5 GHz from JD $=$ 2449874.470 to JD $=$ 2449875.408. In this case we obtain an even higher brightness temperature of 1.3×10^{17} K.

Many works have been devoted to the study of the possible correlation between the optical and radio emissions in blazars, but no firm conclusion has been derived up to now, mainly because of the inadequate sampling of data. Studies on short-term variations by Wagner et al. (1990, 1993) show correlations. As for long-term variations, sometimes optical and radio flares are seen simultaneously (see e.g. Tornikoski et al. 1994a, 1994b). In other cases radio events have been recognized with a time delay with respect to optical ones: in 10 out of 22 sources observed over many years Tornikoski et al. (1994a) found radio–optical correlations with lags from 0 to several months; similar conclusions were derived by Clements et al. (1995): nine of the eighteen AGNs for which they could obtain a reliable application of the discrete correlation function analysis showed correlations with 0–14 month lags; Hufnagel & Bregman (1992) analysed the variability of five blazars in the B band and at 14.5, 8, and 4.8 GHz over several years and concluded that a weak correlation can be found, with a radio time delay of roughly 1 year; more recently, the analysis of the optical and radio light curves of Mkn 421 around the 1996–97 outburst suggested a temporal lag of 1 month (Tosti et al. 1998). Finally, optical flares have been observed with no radio counterparts, as in the case of AO 0235+16 (Takalo et al. 1998) or the 1994 optical outburst of OJ 287 (see discussion in Valtaoja 1998).

A comparison between the optical fluxes in the R band and the radio ones is shown in Figs. 11 and 12. The optical fluxes have been derived by first correcting magnitudes for the Galactic extinction using a value of 0.23 mag in the B band (from NED) and the law of Cardelli et al. (1989), and then applying the absolute flux calibration by Bessell (1979).

From an inspection of Figs. 11 and 12 one can see that there are no signs of an increased radio emission in correspondence to the two last optical observational seasons, and in particular during the 1998 outburst. However, the fact that a radio outburst is not seen simultaneously with the optical one still leaves the possibility that an increased radio flux can be seen with a time delay open. Unfortunately, the non-intensive radio sampling does not allow a significant correlation analysis between optical and radio emissions.

8. The spectral energy distribution

The spectral energy distribution (SED) of S4 0954+65 resembles those of flat-spectrum radio quasars, with the synchrotron emission peaking in the IR–optical band and a flat X-ray spectrum suggesting an inverse-Compton origin of the X-ray flux (see e.g. Sambruna et al. 1996).

Fig. 13 shows the SED of 0954+658 from the radio to the X-ray band: data are from NED, Steppe et al. (1988), Impey & Neugebauer (1988), Sambruna et al. (1996), Taylor et al. (1996), Lamer et al. (1996), Comastri et al. (1997), the Metsähovi Radio Observatory, and the UMRAO database; optical data are

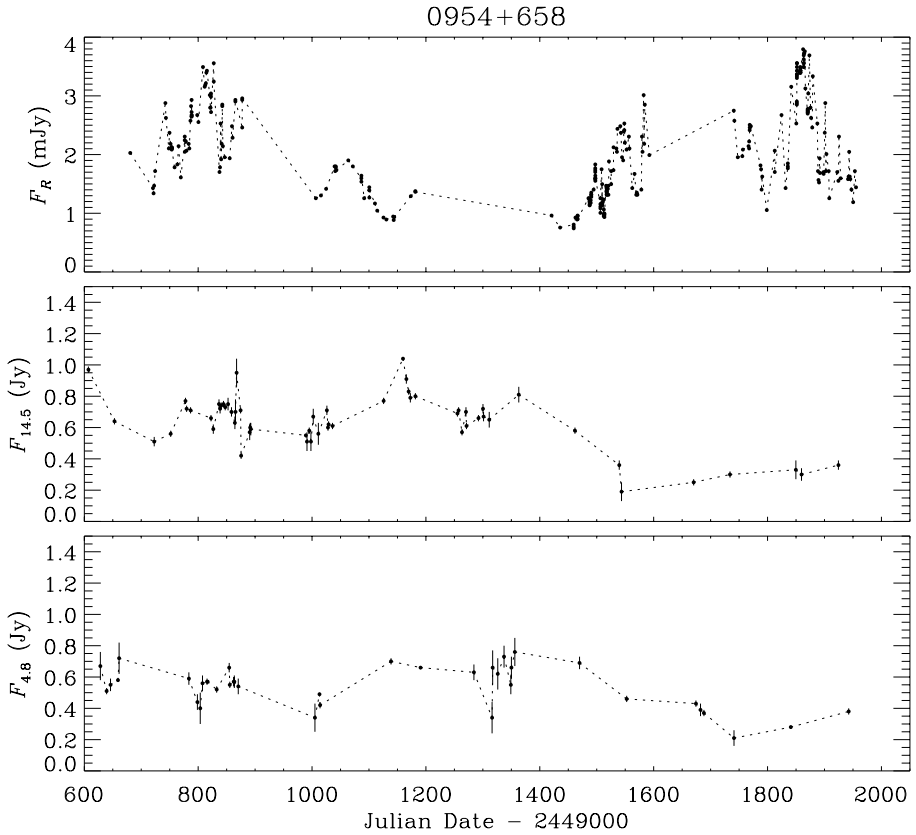

Fig. 12. Confrontation between the optical data in the R band (top panel) and the radio data at 14.5 GHz (middle panel) and 4.8 GHz (bottom panel) from the UMRAO database

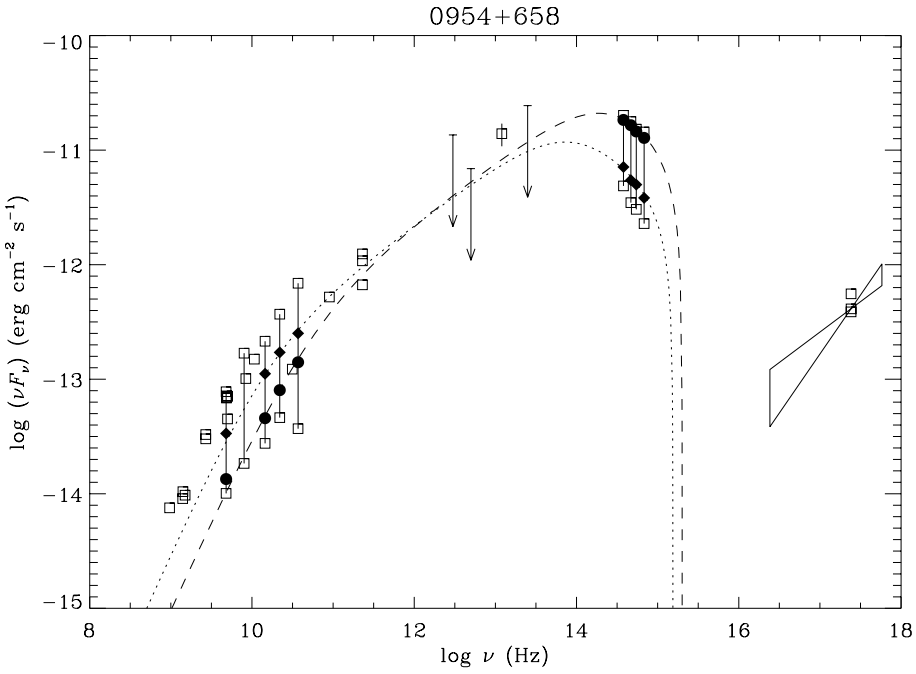

Fig. 13. The spectral energy distribution of S4 0954+65 from the radio to the X-ray band; the ranges of flux variation in the radio and optical bands are shown by solid lines; the upper limits to the 12, 60, and 100 μm fluxes are indicated by arrows; filled circles (diamonds) correspond to contemporaneous radio–optical data during a high (low) optical state; dotted and dashed lines are theoretical fits obtained with a helical-jet model

from this work. The X-ray spectrum is plotted according to the spectral index derived by Comastri et al. (1997): $\alpha = 0.23^{+0.24}_{-0.26}$.

We have indicated the maximum and minimum fluxes in $BVRI$ we observed over the four monitoring years: the range of flux variation for each band is displayed by a solid line. Analogously, we have reported the maximum and minimum radio fluxes at 22 and 37 GHz detected by the Metsähovi Radio Observatory in the last 10 years and those at 4.8, 8.0, and 14.5 GHz registered by the UMRAO over the last 14 years. Again, the spread of the data is indicated by solid lines.

A meaningful theoretical interpretation of the SED requires that simultaneous data be fitted by the model. To this end we

have plotted with filled symbols the optical data corresponding to a high (JD $= 2450863$, circles) and a low (JD $= 2450110$, diamonds) optical state, together with the contemporaneous radio data at 4.8 and 14.5 GHz from the UMRAO database and at 22 and 37 GHz from Metsähovi. The radio data are not exactly simultaneous with the optical ones, but were taken within a few days from them. One can see that a low radio state corresponds to the high optical state, whereas the source presented a high radio level during the low optical state. We are not claiming that a general anticorrelation between optical and radio data does exist: low (high) optical states can be found corresponding to low (high) radio states. But we think that anticorrelated states can better constrain models.

In the following, two different models will be applied to the above discussed SEDs of S4 0954+65: the former is a steady-flux model, which explains brightness variations in terms of a change of the jet orientation with respect to the line of sight; the latter is a homogeneous model, according to which flux variations are the result of changes in the intrinsic power.

8.1. Helical-jet model

The non-thermal emission from blazars is usually interpreted as synchrotron radiation produced in a magnetized plasma and relativistically beamed toward us. Different models consider the emitting region as either a homogeneous sphere or an inhomogeneous jet and energetic processes are invoked to explain the observed flux variations. These models have recently been challenged by the extraordinary X-ray brightness of Mkn 501 detected by the Satellite per Astronomia X "Beppo" (BeppoSAX) (Pian et al. 1998; Ghisellini 1998). An alternative scenario which fairly accounts for the Mkn 501 behaviour has been suggested by Villata & Raiteri (1999). In their picture the synchrotron emission is produced inside an inhomogeneous jet, which is bent in a helical shape because of the orbital motion of the parent black hole in a binary black hole system. The highest-frequency synchrotron radiation is produced closer to the jet apex, while the softer one comes from farther on. According to this model, flux variations at a given wavelength occur when there is a change in the viewing angle of the jet segment(s) emitting that wavelength, because of relativistic beaming, without the need of postulating intrinsic energetic processes. Moreover, one can have at the same time a flux enhancement at a given frequency and a flux depletion in another band, because of the different orientation of the corresponding production sites inside the jet.

It has to be noted that helical jets have been diffusely discussed in the literature, on both observational and theoretical points of view (see references in Villata & Raiteri 1999; in particular, see also Zensus 1997; Roos 1988; Kaastra & Roos 1992; Camenzind & Krockenberger 1992; Schramm et al. 1993; Wagner et al. 1995; Steffen et al. 1995). As noted in Sect. 2, radio maps of S4 0954+65 show a curved jet.

In the following we apply the model by Villata & Raiteri (1999) to the case of S4 0954+65.

Each slice of the jet emits a range of frequencies between $\nu'_{\rm min}$ and $\nu'_{\rm max}$ in the plasma rest reference frame (primed frequencies refer to this frame). These are supposed to decrease with increasing distance from the jet apex l:

$$\nu'_{\rm min}(l) = \nu'_{\rm min}(0)\left(1+\frac{l}{l_1}\right)^{-c_1}, \quad c_1>0\,, \tag{1}$$

$$\nu'_{\rm max}(l) = \nu'_{\rm max}(0)\left(1+\frac{l}{l_2}\right)^{-c_2}, \quad c_2>0\,, \tag{2}$$

where the non-dimensional length l is given in units of the length of the cylindrical-helix axis (z-axis), i.e. such that $l_{\rm max}=\sec\zeta$ at $z_{\rm max}=1$, being ζ the helix pitch angle; $\nu'_{\rm min}(0)$ and $\nu'_{\rm max}(0)$ are the values at $l=z=0$, l_1 and l_2 are length scales. In the following we assume that $\nu'_{\rm min}(0)=\nu'_{\rm max}(0)=\nu'_0$.

The choice of a cylindrical helix is the simplest one; other more complicated shapes (e.g. conical, paraboloidal, etc.) would introduce other parameters into the model and would not be more justified by observations of VLBI jets, which do not show any enlargement of the structure on the small scales we are concerned with. A superimposition of another helical distortion is possible on much larger scales, as due to the precession motion of the black hole spin axis, and this could be conical rather than cylindrical, but out of the closest-to-the-apex and strongly-emitting zone of interest (see Villata & Raiteri 1999). In any case, a different configuration (e.g. conical instead of cylindrical) would give the same results by changing the parameters in Eqs. (1) and (2), i.e. the inhomogeneity law of the jet, which is even more arbitrary.

The observed flux density at frequency ν coming from a jet slice of thickness $\mathrm{d}l$ is

$$\mathrm{d}F_\nu(\nu) \propto \delta^3 \nu^{-\alpha_0}\,\mathrm{d}l\,, \tag{3}$$

where α_0 is the power-law index of the local synchrotron spectrum, and

$$\delta = [\gamma(1-\beta\cos\theta)]^{-1} \tag{4}$$

is the beaming or Doppler factor, β being the bulk velocity of the emitting plasma in units of the speed of light, $\gamma=(1-\beta^2)^{-1/2}$ the corresponding Lorentz factor, and θ the angle between the velocity vector and the line of sight. The angle θ (and hence δ) varies along the jet as

$$\cos\theta(z) = \cos\psi\cos\zeta + \sin\psi\sin\zeta\cos[\phi-\varphi(z)]\,, \tag{5}$$

where ψ is the angle between the z-axis and the line of sight, ϕ is the azimuthal difference between the line of sight and the initial direction of the helix, $\varphi(z)$ is the azimuthal angle covered by the helical path at z.

The total flux density at frequency ν coming from the whole jet is obtained by integrating along all the portions that contribute to that observed frequency:

$$F_\nu(\nu) \propto \nu^{-\alpha_0}\sec\zeta\sum_i\int_{\Delta z_i(\nu)}\delta^3(z)\,\mathrm{d}z\,, \tag{6}$$

where $\Delta z_i(\nu)$ are the z intervals corresponding to the jet segments emitting the observed frequency ν along the line of sight, i.e. where the condition

$$\delta(z)\nu'_{\rm min}(z) \le \nu \le \delta(z)\nu'_{\rm max}(z) \quad (7)$$

is verified.

The proportionality constant in Eq. (6) is considered independent of time, i.e. intrinsic variations of the flux are not allowed.

The model fits are plotted in Fig. 13; they have been derived with $\log l_1 = -3.2$, $\log l_2 = -1.6$, $c_1 = c_2 = 2.5$, $\log \nu'_0 = 14.3$, $\alpha_0 = 0.5$, $\gamma = 10$, $\zeta = 30°$. The fit to the high optical state has been obtained with $\psi = 25°$, $\phi = 6°$, $\varphi_{\rm max} = 280°$, while the low optical state has $\psi = 24°$, $\phi = 9°$, $\varphi_{\rm max} = 220°$. Hence, the two SEDs are reproduced by only varying the geometrical conditions under which the jet is observed. Obviously, any other intermediate radio–optical state (e.g. high–high, low–low) between these two extreme examples can be "geometrically" fitted as well.

The above set of parameters has been deduced by first constraining α_0 and γ to reasonable values; the ν'_0 value is set by the optical spectrum, and the remaining parameters (not having particular physical constraints) are the result of the fits, which are rather sensitive to their values. In particular, it can be seen how small angle changes modify the SED shape. The needed variation of $1°$ in ψ could be the signature of the precession motion.

The two model fits match the observational data from the radio to the optical band fairly well; the X-ray emission is not accounted for by this synchrotron model, as expected, since an inverse-Compton process is thought to intervene. The study of the implications of this "geometrical" interpretation for the high-energy part of the SED is still under way. In any case, it would not be of extreme interest because of the lack of simultaneous X-ray data.

8.2. Homogeneous models

Ghisellini et al. (1998; hereafter G98) fitted the SEDs of all blazars detected by EGRET for which some spectral information were available in the γ-ray energy band. S4 0954+65 was among those sources, but the fitted data were taken from the literature, and were not simultaneous. It is therefore interesting to check if a fit along the same lines as in G98, but using the data presented in this paper, yields different results. Note in particular that in G98 the optical spectral shape was unknown. This is important, since the steep optical spectrum requires the synchrotron peak to be at lower frequencies, constraining the model.

We have then used the same homogeneous model described in G98, allowing also for the presence of external photons contributing to the inverse-Compton scattering, distributed in frequency as a diluted blackbody peaking at 10^{15} Hz. We have also tried to fit the high optical state together with the hard X-ray and γ-ray spectra, even if all these components were not observed simultaneously (in particular, the γ-ray data refer to the EGRET detection of June–July 1993; Mukherjee et al. 1995). Due to the limited EGRET sensitivity, the detected γ-ray emission may in fact correspond to a bright optical state of the source.

Variability time scales as measured in the optical, X-ray, and γ-ray bands (for blazars in general and S4 0954+65 in particular) imply that the region emitting the flux in these bands is compact. This implies, if the emission is due to the inchoerent synchrotron process, that the radio emission is self-absorbed. In the case of an isotropic population of relativistic electrons with a power-law distribution $N(\gamma) = K\gamma^{-p}$, the self-absorption frequency is given by

$$\nu_{\rm t} = \frac{\delta\nu_B}{1+z} \times \left[\frac{3^{p/2}\pi\sqrt{3\pi}\Gamma(\frac{3p+22}{12})\Gamma(\frac{3p+2}{12})\Gamma(\frac{p+6}{4})}{4\Gamma(\frac{p+8}{4})}\frac{e\tau}{B\sigma_{\rm T}}\right]^{\frac{2}{p+4}} \quad (8)$$

where $\nu_B = 2.8\times10^6\,B$ Hz is the cyclotron frequency, $\tau \equiv \sigma_{\rm T}KR$, and p is the slope of the electron distribution appropriate for those electrons radiating at the self-absorption frequency. In the homogeneous synchrotron self-Compton (SSC) model, the optical depth τ is approximately the ratio of the self-Compton and the synchrotron flux at the same frequency. From the SED shown in Fig. 14 one can estimate $\tau \sim 10^{-4}$, by extrapolating the X-ray spectrum at lower frequencies. The weak dependence of $\nu_{\rm t}$ on τ mitigates the uncertainty related to this rather rough estimate. With $p = 2$ and $\tau = 10^{-4}\,\tau_{-4}$ in Eq. (8), we obtain $\nu_{\rm t} \sim 240(\delta/10)\tau_{-4}^{1/3}B^{2/3}(1+z)^{-1}$ GHz. Unless the magnetic field is exceptionally small, the radio flux is self-absorbed. Then we need another component (with a lower magnetic field and a smaller τ) to account for the observed far-IR and radio emissions. This additional region would necessarily be larger, and will not account for the observed fast radio variability. Indeed, any inchoerent synchrotron model faces severe problems in explaining intraday radio variability (see for a review Wagner & Witzel 1995), not only because of the large brightness temperatures, but also because of self-absorption.

The results are shown in Fig. 14, where the dashed and dotted lines refer to the two simultaneous radio–optical sets of data: State 1 corresponds to the high-optical and low-radio state, and State 2 to the low-optical and high-radio one. We have tried to change the minimum number of parameters to account for both states. The used input parameters are listed in Table 3. The dimension of the emitting regions has been kept fixed to $R = 2\times10^{16}$ cm for the compact region responsible for the bulk of the emission, and to $R = 7\times10^{17}$ cm for the more extended, radio-emitting region. As mentioned above, the emission from this large region is not meant to be responsible for the observed fast radio variability. It shows the contribution of the inchoerent synchrotron process originating in a larger part of the jet, above which the mechanism producing the intraday variations has to contribute. The beaming factor has been kept fixed to $\delta = 15$. Throughout the region, assumed spherical, the intrinsic power $L'_{\rm inj}$ is injected continuously in the form of relativistic electrons, distributed in energy as a power law of slope s between $\gamma_{\rm min}$ and $\gamma_{\rm max}$. The magnetic field B is assumed to be homogeneous and

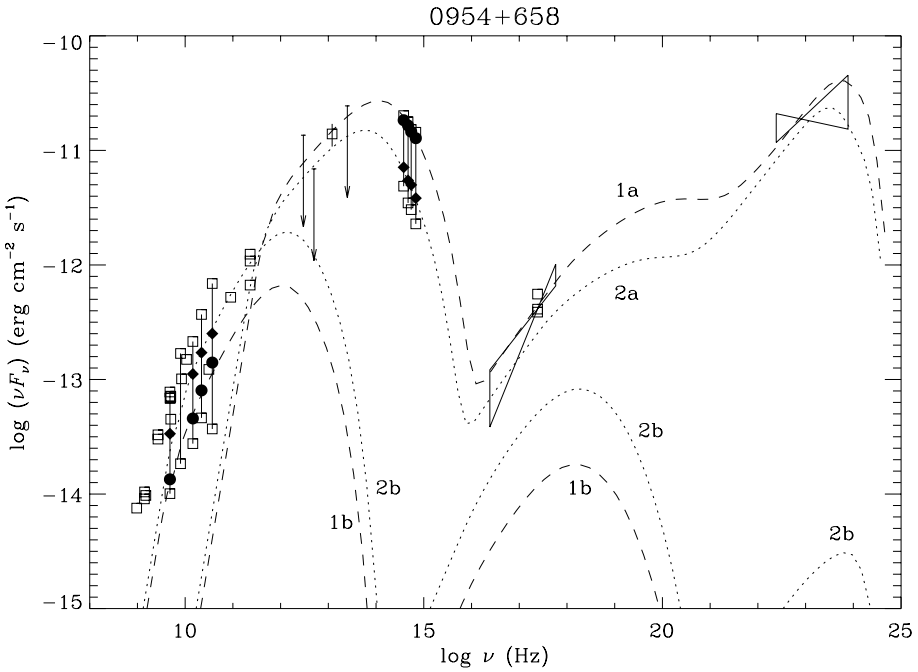

Fig. 14. The SED of S4 0954+65 (filled symbols refer to simultaneous optical and radio data) has been fitted with homogeneous synchrotron and inverse-Compton models as described in the text (dashed and dotted lines). The radio to far-infrared part of the spectrum originates in a region different from (and larger than) the one responsible for the bulk of the emission. The bumpy structure of the high-energy emission is due to the contribution of two components: in the X-ray band the synchrotron self-Compton (SSC) emission dominates, while the higher-energy flux is dominated by scattering between electrons and photons produced externally (EC). The curves in any case show the sum of the SSC and EC components. Labels correspond to the models in Table 3. The two bottom curves between about 10^{15} and 10^{20} Hz are the first-order self-Compton emissions of the two larger regions. The bottom dotted curve at $\sim 10^{23}$–10^{24} Hz is the second-order self-Compton emission of one of the large regions

Table 3. Input parameters for homogenous external-Compton models

State	region	R (cm)	$\ell'_{\rm inj}$	$\ell'_{\rm ext}$	$L'_{\rm inj}$ (erg s^{-1})	B (Gauss)	$\gamma_{\rm min}$	$\gamma_{\rm max}$	s	label
1	compact	2×10^{16}	7×10^{-3}	2.3×10^{-2}	5.2×10^{42}	2.2	1.25×10^{3}	5×10^{3}	3.6	1a
	large	7×10^{17}	2×10^{-5}		5.2×10^{41}	0.02	10^{3}	4×10^{3}	3.8	1b
2	compact	2×10^{16}	4×10^{-3}	2.3×10^{-2}	2.9×10^{42}	2.2	9×10^{2}	4×10^{3}	3.8	2a
	large	7×10^{17}	3.6×10^{-5}		9.3×10^{41}	0.027	10^{3}	4×10^{3}	3.8	2b

tangled. The injected power and the source dimension combine to give the dimensionless compactness parameter, defined as $\ell \equiv L\sigma_{\rm T}/(Rm_{\rm e}c^3)$, which is reported in Table 3. In this way we can easily compare the injected compactness with the compactness (as seen in the comoving frame) of the external radiation, $\ell'_{\rm ext}$ (see G98 for a more detailed discussion).

As can be seen in Fig. 14, the EGRET spectrum is hard, indicating that the peak of the high-energy emission is around or above 1 GeV. On the other hand, the steep optical spectrum indicates that the synchrotron component of the spectrum peaks below the optical band. The energy separation of the two peaks is therefore very large, difficult to explain in the pure SSC model (see e.g. Ghisellini et al. 1996), and instead indicating the presence of seed photons, produced externally to the jet, of typical frequencies larger than the peak synchrotron frequency. The high-energy spectrum of S4 0954+65 is therefore the sum of two components: the SSC component dominates the emission in the soft and medium-energy X-ray band, while the external-Compton (EC) component dominates at larger energies, especially in the EGRET band. This is the reason of the "bumpy" high-energy spectrum of Fig. 14.

The values of the parameters derived in this paper are consistent with the ones derived by G98 in the case of the EC model, but now the steep optical spectrum (not available in the G98 paper) strengthens the conclusion that some amount of EC is indeed required. As can be seen in Fig. 1 of G98, a pure SSC model has also some difficulties to explain both the X-ray and the γ-ray spectrum and requires much larger electron energies (electrons emitting at the peaks of the emission should have $\gamma \sim 10^5$) and, correspondingly, a lower value of the magnetic field ($B \sim 0.02$ Gauss for the compact component).

As pointed out in Comastri et al. (1995), the source of external photons for the inverse Compton scattering process is somewhat problematic, since the emission lines in this source are particularly weak (as reported by Stickel et al. 1993). However, other sources of external photons cannot be excluded: some scattering material outside the jet may scatter some fraction of the accretion-disk radiation, while scattering material within the jet (or close to the walls of the jet) can scatter the synchrotron radiation produced by the jet itself. The required amount of external radiation, as measured in the comoving frame, corresponds to a compactness $\ell'_{\rm ext} = 2.3\times10^{-2}$, as listed in Table 3. This translates to a (comoving) radiation energy density

of external photons $U'_{\rm ext} = 0.25\,{\rm erg\,cm^{-3}}$, to be compared with the magnetic energy density $U_B = 0.19\,{\rm erg\,cm^{-3}}$ and with the synchrotron energy density $U'_{\rm syn} = 0.045\,{\rm erg\,cm^{-3}}$. From $U'_{\rm ext} \sim \Gamma^2 L_{\rm ext}/(4\pi R^2 c)$, we derive $L_{\rm ext} \sim 4 \times 10^{42} (R/10^{17}\,{\rm cm})^2\,{\rm erg\,s^{-1}}$.

9. Conclusions

Four years of optical and radio monitoring of the blazar S4 0954+65 have produced a large amount of data, which can give information about the source variability on both short and long time scales. We detected an overall maximum variation of $2.0\,{\rm mag}$ in the B band, and variations up to some tenths of magnitude in a few hours, confirming that this blazar is very active on short as well as on long time scales.

The radio light curves are not so well sampled; however, a couple of noticeable fast-variability events were detected, requiring high brightness temperatures and Doppler factors.

A comparison between optical and radio data is not able to put in evidence or exclude a possible correlation between the emissions in the two bands, mainly because of the poor radio sampling: the matter remains under debate, but a good radio monitoring would be of great value to see whether a delayed radio outburst follows the optical outburst observed in January–March 1998.

Spectral energy distributions of S4 0954+65 using contemporaneous radio and optical data in which a high optical state is associated with a low radio state and vice versa are well fitted by a steady-emission helical-jet model. This implies that it is not necessary to invoke energetic processes in order to explain the long-term SED variations, which can be interpreted in terms of a geometrical effect, by changing the jet orientation with respect to the observer's line of sight. Such interpretation is in agreement with the appearance of a curved jet in the VLA and VLBI images of S4 0954+65 and with the long-term quasi-achromatic optical variations of this source. The implications of this model on the high-energy part of the SED have not been investigated yet.

On the other side, a homogeneous model can explain the observed radiation from the IR to the γ-rays with a single emission region, but needs a distinct, larger region to account for the radio flux. The application of this model to the SEDs of S4 0954+65 presented in Sect. 8 gives support to the hypothesis that external soft photons to comptonize are required in addition to the local ones in order to explain the EGRET measurements.

It is beyond the aim of this work to perform a more detailed comparison between the two models; the observational data on S4 0954+65 presented in this paper do not allow us to decide which picture is more reliable. A further, more intense observational effort is required before one can put stronger constraints to the theoretical interpretation of blazar variability.

Acknowledgements. This work was partly supported by the Italian Ministry for University and Research (MURST) under grant Cofin98-02-32 and by the Italian Space Agency (ASI), and has made use of:

– the STScI Digitized Sky Survey (DSS);
– the NASA/IPAC Extragalactic Database (NED), which is operated by the Jet Propulsion Laboratory, California Institute of Technology, under contract with the National Aeronautics and Space Administration;
– data from the University of Michigan Radio Astronomy Observatory, which is supported by the National Science Foundation and by funds from the University of Michigan.

References

Aller H.D., Aller M.F., Latimer G.E., Hodge P.E., 1985, ApJS 59, 513
Aller M.F., Aller H.D., Hughes P.A., Latimer G.E., 1999, ApJ 512, 601
Bessell M.S., 1979, PASP 91, 589
Camenzind M., Krockenberger M., 1992, A&A 255, 59
Cardelli J.A., Clayton G.C., Mathis J.S., 1989, ApJ 345, 245
Catanese M., Borione A., Covault C.E., et al., 1996, ApJ 469, 572
Clements S.D., Smith A.G., Aller H.D., Aller M.F., 1995, AJ 110, 529
Cohen A.M., Porcas R.W., Browne I.W.A., et al., 1977, Mem. R. Astron. Soc. 84, 1
Comastri A., Molendi S., Ghisellini G., 1995, MNRAS 277, 297
Comastri A., Fossati G., Ghisellini G., 1997, ApJ 480, 297
Fiedler R., Dennison B., Johnston K., Hewish A., 1987, Nat 326, 675
Gabuzda D.C., Cawthorne T.V., 1996, MNRAS 283, 759
Gabuzda D.C., Cawthorne T.V., Roberts D.H., Wardle J.F.C., 1992, ApJ 388, 40
Gabuzda D.C., Mullan C.M., Cawthorne T.V., Wardle J.F.C., Roberts D.H., 1994, ApJ 435, 140
Ghisellini G., 1998, In: Scarsi L., Bradt H., Giommi P., Fiore F. (eds.) The Active X-Ray Sky. Nucl. Phys. B (Proc. Suppl.) 69, 397
Ghisellini G., Maraschi L., Dondi L., 1996, A&AS 120, 503
Ghisellini G., Celotti A., Fossati G., Maraschi L., Comastri A., 1998, MNRAS 301, 451 (G98)
Heidt J., Wagner S.J., 1996, A&A 305, 42
Hufnagel B.R., Bregman J.N., 1992, ApJ 386, 473
Impey C.D., Neugebauer G., 1988, AJ 95, 307
Kaastra J.S., Roos N., 1992, A&A 254, 96
Kollgaard R.I., Wardle J.F.C., Roberts D.H., Gabuzda D.C., 1992, AJ 104, 1687
Kuhr H., Witzel A., Pauliny-Toth I.I.K., Nauber U., 1981, A&AS 45, 367
Lamer G., Brunner H., Staubert R., 1996, A&A 311, 384
Landolt A.U., 1992, AJ 104, 340
Lawrence C.R., Pearson T.J., Readhead A.C.S., Unwin S.C., 1986, AJ 91, 494
Mukherjee R., Aller H.D., Aller M.F., et al., 1995, ApJ 445, 189
Mukherjee R., Bertsch D.L., Bloom S.D., et al., 1997, ApJ 490, 116
Padovani P., Giommi P., 1995, MNRAS 277, 1477
Pian E., Vacanti G., Tagliaferri G., et al., 1998, ApJ 492, L17
Quirrenbach A., Witzel A., Krichbaum T.P., et al., 1992, A&A 258, 279
Roos N., 1988, ApJ 334, 95
Sambruna R.M., Maraschi L., Urry C.M., 1996, ApJ 463, 444
Schramm K.-J., Borgeest U., Camenzind M., et al., 1993, A&A 278, 391
Steffen W., Zensus J.A., Krichbaum T.P., Witzel A., Qian S.J., 1995, A&A 302, 335
Steppe H., Salter C.J., Chini R., et al., 1988, A&AS 75, 317
Stickel M., Padovani P., Urry M., Kuhr H., 1991, ApJ 374, 431
Stickel M., Fried J.W., Kuhr H., 1993, A&AS 98, 393
Takalo L.O., Sillanpää A., Valtaoja E., et al., 1998, A&AS 129, 577

Taylor G.B., Vermeulen R.C., Readhead A.C.S., et al., 1996, ApJS 107, 37
Teräsranta H., Tornikoski M., Valtaoja E., et al., 1992, A&AS 94, 121
Tornikoski M., Valtaoja E., Teräsranta H., et al., 1994a, A&A 289, 673
Tornikoski M., Valtaoja E., Teräsranta H., Okyudo M., 1994b, A&A 286, 80
Tosti G., Pascolini S., Fiorucci M., 1996, PASP 106, 706
Tosti G., Fiorucci M., Luciani M., et al., 1998, A&A 339, 41
Urry C.M., Sambruna R.M., Worrall D.M., et al., 1996, ApJ 463, 424
Valtaoja E., 1998, In: Tosti G., Takalo L. (eds.) Proc. OJ-94 Annual Meeting 1997, Multifrequency Monitoring of Blazars. Pubblicazioni Osservatorio Astronomico Università di Perugia, Perugia, vol. 3, p. 62
Véron-Cetty M.-P., Véron P., 1993, A Catalogue of Quasars and Active Nuclei. ($6^{\rm th}$ Edition), ESO Scientific Report 13
Villata M., Raiteri C.M., 1999, A&A 347, 30
Wagner S.J., Witzel A., 1995, ARA&A 33, 163
Wagner S.J., Sanchez-Pons F., Quirrenbach A., Witzel A., 1990, A&A 235, L1
Wagner S.J., Witzel A., Krichbaum T.P., et al., 1993, A&A 271, 344
Wagner S.J., Camenzind M., Dreissigacker O., et al., 1995, A&A 298, 688
Walsh D., Beckers J.M., Carswell R.F., Weymann R.J., 1984, MNRAS 211, 105
Waltman E.B., Fiedler R.L., Johnston K.J., et al., 1991, ApJS 77, 379
Wurtz R., Stocke J.T., Yee H.K.C., 1996, ApJS 103, 109
Zensus J.A., 1997, ARA&A 35, 607